The Journal of Chemical Physics

Free energy of adhesion of lipid bilayers on titania surfaces

Cite as: J. Chem. Phys. **151**, 134707 (2019); https://doi.org/10.1063/1.5120810
Submitted: 21 July 2019 . Accepted: 09 September 2019 . Published Online: 03 October 2019

M. Schneemilch, and N. Quirke

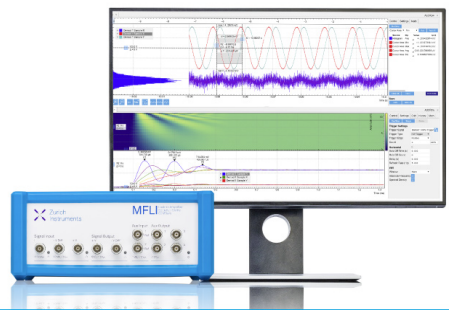

The Journal of Chemical Physics ARTICLE scitation.org/journal/jcp

Free energy of adhesion of lipid bilayers on titania surfaces

Cite as: J. Chem. Phys. 151, 134707 (2019); doi: 10.1063/1.5120810
Submitted: 21 July 2019 • Accepted: 9 September 2019 •
Published Online: 3 October 2019

M. Schneemilch and N. Quirke[a)]

AFFILIATIONS

Department of Chemistry, Imperial College London, London SW7 2AY, United Kingdom

[a)]Author to whom correspondence should be addressed: n.quirke@ic.ac.uk

ABSTRACT

The adhesion strength between a flexible membrane and a solid substrate (formally the free energy of adhesion per unit area) is difficult to determine experimentally, yet is a key parameter in determining the extent of the wrapping of a particle by the membrane. Here, we present molecular dynamics simulations designed to estimate this quantity between dimyristoylphosphatidylcholine (DMPC) bilayers and a range of low-energy titanium dioxide cleavage planes for both anatase and rutile polymorphs. The average adhesion strength across the cleavage planes for rutile and anatase is relatively weak $\sim -2.0 \pm 0.4$ mN m^{-1}. However, rutile has two surfaces (100 and 101) displaying relatively strong adhesion (-4 mN m^{-1}), while anatase has only one (110). This suggests a slightly greater tendency for bilayers to wrap rutile particles compared to anatase particles but both would wrap less than amorphous silica. We also estimate the adsorption free energies of isolated DMPC lipids and find that only the rutile 101 surface shows significant adsorption. In addition, we estimate the adhesion enthalpies and infer that the entropic contribution to the adhesion free energy drives adhesion on the rutile surfaces and opposes adhesion on the anatase surfaces.

I. INTRODUCTION

The interaction of inorganic surfaces with biological tissue is of interest in medicine and in toxicology. In particular, the effects of exposure to finely divided inorganic materials in the form of nanoparticles are of great concern[1–5] as their toxicological properties are uncertain, even for naturally occurring minerals such as silica and titania. There has been a rapid increase in the number and variety of engineered nanoparticles in the environment,[6] for example, those arising from the use of batteries, catalysts, chemical coatings and paints, packaging, electronic devices, implants, biomedicines, food additives, and cosmetics.[7] Nanoparticles may be encountered in humans through inhalation, digestion, and injection or through direct contact with the skin. Our research[8,9] is focused on the interaction of nanoparticles with cytoplasmic membranes with a view to assessing the likely damage due to nanoparticles at the cellular level.[10] To help identify the essential features of such interactions, we first study much simpler "model" membranes such as lipid vesicles.[11,12]

A key measure of the degree of interaction between nanoparticles and membranes is the extent to which the nanoparticle adheres to or is wrapped by the membrane. According to the Helfrich membrane model[13] applied by Deserno and Gelbart[14] to the wrapping of spherical particles by membranes, this is determined by whether the adhesion strength is sufficient to overcome the bending energy associated with membrane deformation during particle wrapping. Particles smaller than a critical size will not adhere to the membrane. Larger particles will adhere and undergo wrapping; the extent to which wrapping occurs is determined by the membrane tension. With low tension and/or strong adhesion, particles will be completely engulfed, following which the particle detaches from the membrane leaving a membrane pore through which cytosol leakage can occur. The adhesion strength drives the particle wrapping process, and therefore, any assessment of the potential nanotoxicity of a material must include an estimate of its adhesion strength for a given membrane which may be approximated by the adhesion strength with respect to the membrane lipids. Adhesion strength data can then be used to develop models of *passive* nanoparticle uptake by human cells as well as pulmonary surfactant disruption due to the presence of nanoparticles in the alveolar spaces of lungs. A major obstacle to progress is the almost complete lack of quantitative experimental data for nanoparticle/lipid bilayer adsorption

enthalpies and free energies (adsorption strength).[15] One solution is to calculate such data using molecular simulation, and indeed, in previous work, we have calculated adhesion strengths for dimyristoylphosphatidylcholine (DMPC) bilayers on planar surfaces of both gold[16] and silica.[17]

We found that silanols on a range of different silica surfaces formed hydrogen bonds with water molecules and that the water immersion enthalpy for all surfaces varied linearly with the surface density of these hydrogen bonds. The adhesion strength of DMPC bilayers was found to be a linear function of the surface density of hydrogen bonds formed between silanols and the lipid molecules on crystalline surfaces. Approximately 20% of isolated silanols formed such bonds, but more than 99% of mutually interacting geminal silanols did not. On amorphous silica, the bilayer displayed much stronger adhesion than expected from the crystalline surface data, consistent with toxicity data for silica.

In the present paper, we expand our study to consider titanium dioxide, or titania, surfaces. Titania is a major additive for paints, sunscreens, cosmetics, toothpastes, pharmaceuticals, paper, and food, adding whiteness, brightness, UV protection, and resistance to discoloration. Millions of tons of titanium dioxide are produced globally each year, 70% of which is used for paints. Although considered to be a safe material in conventional form, at the nanoscale, its toxicity is unknown. A significant fraction of nano-sized titania has been identified in food and personal care products.[18]

Titania nanoparticles have been reported to produce toxic effects in experimental animals,[5,19] including DNA damage as well as genotoxicity, lung inflammation,[20] oxidative stress,[21] and endothelial cell leakiness[22] which we might expect to be reflected in strong adhesion of lipid bilayers on titania and vesicle rupture. However, experimental studies[23] have shown that POPC vesicles are adsorbed on, but *not ruptured* by, titania surfaces. Similarly, when exposed to titania nanoparticles (20 nm and 50 nm), PC liposomes do not fuse onto the TiO_2 surface[24] due to strong water adsorption at the titania surface (see later). A study[25] of the cytotoxicity of fourth period metal oxide nanoparticles including TiO_2 on non-transformed human lung cells (BEAS-2B) and human bronchoalveolar carcinoma-derived cells (A549) concluded that the response to NP exposure based on particle mass dosimetry could be categorized into three toxicity groups: none to minimal (TiO_2, Cr_2O_3, and Fe_2O_3), moderate dose dependent (Mn_2O_3 and NiO), and strong and steep (CuO and ZnO). On the other hand, 10 nm diameter anatase nanotubes (lengths of hundreds of nanometers) have been reported to interact strongly with lipid vesicles (mainly DOPC) and live lung epithelial cell layer (LA-4 cells) sequestering lipids and proteins, disrupting the integrity of the membrane.[26] Finally, we note that toxicity studies do not always differentiate between the different forms of titania. Experiments measuring the disruption of DMPC monolayers supported on mercury electrodes have shown a greater membranolytic activity for anatase particles compared to rutile.[27] Yu *et al.*[28] found that anatase and rutile TiO_2 nanoparticles of similar size and zeta potential have different toxicity for organelles in macrophages, arising from their different affinity to proteins and phospholipids. Anatase nanoparticles had a high affinity for proteins, whereas rutile nanoparticles had a high affinity for the phospholipid and PE (phosphatidylethanolamine) and targeted the plasma and lysosome membranes, causing reactive oxygen species (ROS)-independent necrotic cell death.

In the absence of quantitative experimental data for lipid bilayer adsorption on titania, molecular dynamics simulation offers an alternative route to increasing our understanding which may be of use in resolving a confusing situation. In what follows, we simulate DMPC lipid bilayers on a range of anatase and rutile titania surfaces. We use a force field for titania[29] developed on the basis of density functional theory (DFT) simulations.[30] It is able to reproduce the empirically determined structural properties and the water adsorption enthalpy. In addition, it accurately reproduces the surface water density profile generated from DFT simulation. Using this force field, we model bilayer adhesion on four rutile surfaces, with Miller indexes 110, 100, 101, and 001 and four anatase surfaces with indexes 101, 100, 001, and 110. These represent low energy surfaces of two common polymorphs of titania.[31]

II. METHODOLOGY

The DMPC lipids were modeled using the fully atomistic 118 site Slipids force field which was developed for use in conjunction with TIP3P water.[32–34] This system was shown to reproduce many experimentally observed properties of bilayers including the lipid specific area and volume, bilayer thickness, isothermal area compressibility, and nuclear magnetic resonance (NMR) order parameters and scattering form factors.

The titania force field was developed by the Lyubartsev group in Stockholm. The force field was derived from the electron densities generated by DFT simulation[30] and was able to reproduce the DFT surface water density profiles and empirically determined water adsorption enthalpies. These simulations also showed that no hydroxyls were formed on the titania surfaces, with the exception of the rutile 001 and anatase 001 surfaces. The configurations used to simulate these two surfaces were taken from the DFT simulations and consequently have some OH groups bonded on the surface. Larger slabs were generated from the DFT configurations by tiling. All the other surfaces were constructed by cleaving the bulk crystal and have only physisorbed water. Interaction potentials between lipids and titania were generated with Lorentz-Berthelot mixing rules.

All simulations were performed using GROMACS 2016.4 software with a 2 fs time step. Temperatures were maintained at 310 K using the Nose-Hoover thermostat with 5 ps time constant. Pressure was maintained at 1 atm using an anisotropic Parrinello-Rahman barostat with 10 ps time constant. Electrostatic interactions were calculated with a Particle Mesh Ewald (PME) summation. Lennard-Jones and real space electrostatic interaction potentials were truncated at 1.4 nm. Error estimates were obtained by block averaging unless stated otherwise. Where no errors are recorded, the uncertainty was smaller than the last significant figure in the reported value.

A. Heat of immersion

The change in enthalpy upon immersion was estimated by conducting simulations of three systems: the surface in contact with water, the surface in vacuum, and a simulation of bulk water containing an identical number of water molecules as the first system. The immersion enthalpy, ΔH_{imm}, was then calculated using the following equation:

$$\Delta H_{imm} = \frac{1}{2A}\left(H_{surface-water} - H_{surface-vacuum} - H_{water}\right), \quad (1)$$

where H is the enthalpy of the system and A is the area of the interface. All systems were simulated for 400 ns with 10 ns equilibration.

B. Single lipid adsorption free energy

The adsorption free energy was calculated from potential of mean force simulations. A single DMPC molecule was placed into the water channel, roughly 12 nm wide, formed between periodic images of the TiO_2 slab. Harmonic constraints were applied between the slab surface and the center of mass of the lipid with a force constant of 1000 kJ mol^{-1} nm^{-2}. There were 27 umbrella windows with a grid spacing of 0.1 nm, and each window was simulated for 50 ns. The potential of mean force was calculated using the weighted histogram method.[35]

C. Adhesion strength

Surface slabs were constructed with surface dimensions of approximately 30 × 4 nm. Equilibrated bilayer ribbons were then brought into contact with the titania surfaces. The edges of the ribbon were then maintained at a distance of 8 nm from the titania surface using the GROMACS pull code with a harmonic constraint with force constant of 10 kJ mol^{-1}. A total of 18 lipids comprised the pull group at each edge of the ribbon. The distribution of lipids in the ribbon was maintained at equilibrium by periodically updating the lipids in the pull group, as described in our previous paper.[16] The constraint force, F, required to keep the end of the ribbon at a distance h above the surface was monitored during the simulation. The constraint force is related to the adhesion strength k_w by

$$k_w = F\frac{dh}{dA}, \quad (2)$$

where dA is the increase in the area of the adsorbed bilayer resulting from a reduction in the restraint of height by dh. The ratio dh/dA is the product of twice the inverse of the area per lipid in the supported lipid bilayer and the inverse of dn/dh, where n is the number of lipids in the free section of the bilayer. The ratio dn/dh is estimated from the one dimensional lipid number density profile perpendicular to the surface at the point where the magnitude of the gradient is at the minimum. Note that the adhesion strength can be expected to be independent of the restraint height as long as the length of the ribbon is sufficient to ensure that at least some portion of the adhering ribbon is representative of the "bulk" adhesion density, i.e., is not affected by proximity to the edges.

III. RESULTS

A. Titania-water interface

Estimated properties of the rutile-water interfaces are reported in Table I and properties of the anatase-water interfaces in Table II. All titania surfaces exhibited a large degree of hydrophilicity as reflected in the uniformly exothermic heats of immersion, which were an order of magnitude greater than the silica surfaces studied previously. A far greater range in heat of immersion was observed on the anatase surfaces which varied from 392 mN m^{-1} on the anatase 001 surface to 1176 mN m^{-1} on the anatase 100 surface. In contrast, the heat of immersion on the rutile surfaces varied over a much smaller range, from 847 mN m^{-1} on the rutile 101 surface to 1102 mN m^{-1} on the rutile 001 surface.

The time averaged water-titania hydrogen bond density was also estimated using the GROMACS tool gmx hbond. The hydrogen bond density ranged from 5.85 nm^{-2} to 10.87 nm^{-2} on the rutile 110 and rutile 100 surfaces, respectively. These values are similar to those observed on the silica surfaces. The difference here though

TABLE I. Properties of the rutile-water interfaces.

Polymorph	Rutile	Rutile	Rutile	Rutile
Miller index	110	100	101	001
OH surface density (nm^{-2})	...	...	...	3.42
Solvent accessible area ratio	1.16	1.11	1.03	1.27
Heat of immersion (mN m^{-1})	1024 ± 1	1009 ± 1	847 ± 1	1102 ± 1
Hydrogen bond density (nm^{-2})	5.85	10.87	9.53	10.33
Single lipid adsorption energy (kJ mol^{-1})	−1.8	−3.4	−13.8	−0.4

TABLE II. Properties of the anatase-water interfaces.

Polymorph	Anatase	Anatase	Anatase	Anatase
Miller index	101	100	001	110
OH surface density (nm^{-2})	...	...	4.30	...
Solvent accessible area ratio	1.20	1.01	1.41	1.07
Heat of immersion (mN m^{-1})	774 ± 1	1176 ± 1	392 ± 1	1006 ± 1
Hydrogen bond density (nm^{-2})	6.33	8.66	7.47	8.37
Single lipid adsorption energy (kJ mol^{-1})	−1.7	−0.2	−0.1	−1.9

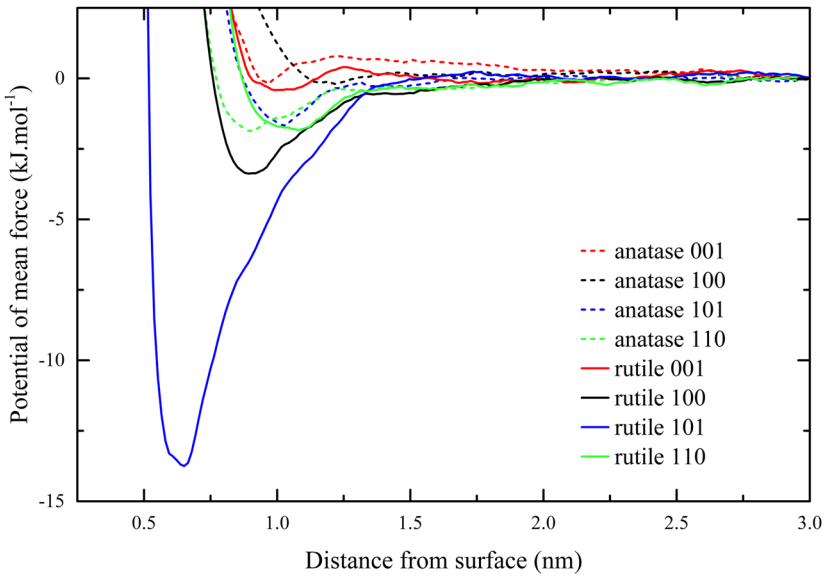

FIG. 1. The adsorption free energy of a single lipid DMPC molecule in aqueous solution on each titania surface.

is that there is no strong correlation between the hydrogen bond density and the heat of immersion. The anatase 001 surface is curious since it has a relatively high OH surface density coupled with a relatively large solvent accessible area ratio yet a meager heat of immersion.

In general, the substrates attract a tightly bound surface water layer and a more loosely bound secondary water layer. The majority of hydrogen bonds are formed between oxygen atoms in the titania surface and water molecules in the second water layer. The exception is the rutile 100 surface, which has a layer of water tightly bound to the substrate with a surface density of 7.1 nm^{-2}. All the water in this layer is hydrogen bonded to the surface, representing the majority of such bonds, with the remaining titania-water hydrogen bonds formed with water in the second layer.

In addition, we measured the free energy of adsorption of single lipids on the titania surfaces. The potentials of mean force (PMFs) for each surface are displayed in Fig. 1, and the free energies of adsorption, corresponding to the minima of each PMF, are recorded in Tables I and II. On the majority of the surfaces, the free energy minimum was less than the available thermal energy, indicating that lipids do not spontaneously adsorb on these surfaces. The only surface to display strong adsorption was the rutile 101 surface with a minimum of −13.8 kJ mol^{-1}. Here, the position of the minimum is significantly closer to the surface compared to the other cleavage planes.

In Fig. 2, an isolated lipid molecule is shown adsorbed on the rutile 101 surface. Also shown, with oxygen atoms in blue, are the physisorbed water molecules. The residence time of these physisorbed molecules is on the nanosecond time scale. The lipid tails adsorb flat to the surface, and the head group protrudes into the bulk water phase. None of the physisorbed water molecules are displaced by the adsorbed lipid, and the negatively charged carbonyl and phosphate groups can engage in favorable short range coulomb interactions with the exposed titanium atoms. However, the single lipid configuration is markedly different to a lipid in an adsorbed bilayer, where only the head group region of the bilayer is in proximity to the surface. For this reason, as shall be seen, the relatively strong adsorption of single lipids on this particular surface is not reflected in the bilayer adhesion strength.

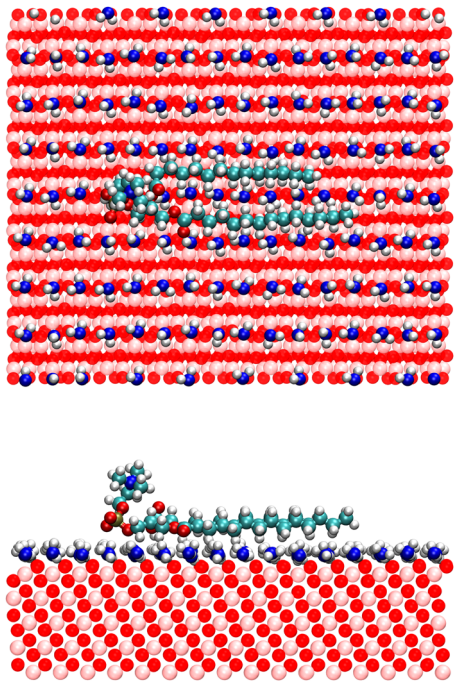

FIG. 2. Top and side views of an isolated DMPC molecule adsorbed on the rutile 101 surface. Physisorbed water molecules are shown with oxygen atoms in blue. All other oxygen atoms are red. Nonphysisorbed water molecules are omitted for clarity.

TABLE III. Properties of the rutile-bilayer interfaces.

Polymorph	Rutile	Rutile	Rutile	Rutile
Miller index	110	100	101	001
ApL (nm^{-2})	0.62	0.65	0.66	0.62
Separation (nm)	1.18	0.89	0.85	0.96
Thickness (nm)	3.20	3.03	3.04	3.16
Adhesion strength ($mN\ m^{-1}$)	−1.8 ± 0.2	−3.6 ± 0.5	−4.0 ± 0.5	−0.3 ± 0.1
Adhesion enthalpy ($mN\ m^{-1}$)	1.6 ± 1.0	2.6 ± 1.1	1.4 ± 1.4	1.9 ± 1.3
Entropic contribution ($mN\ m^{-1}$)	3.5 ± 1.2	6.1 ± 1.6	5.4 ± 2.0	2.2 ± 1.5
Hydrogen bond density (nm^{-2})	5.87	10.11 ± 0.02	9.11 ± 0.01	9.87 ± 0.03

TABLE IV. Properties of the anatase-bilayer interfaces.

Polymorph	Anatase	Anatase	Anatase	Anatase
Miller index	101	100	001	110
ApL (nm^{-2})	0.64	0.63	0.64	0.64
Separation (nm)	1.00	1.53	1.10	0.81
Thickness (nm)	3.08	3.22	3.14	3.12
Adhesion strength ($mN\ m^{-1}$)	−1.0 ± 0.4	−1.1 ± 0.7	−0.6 ± 0.2	−4.0 ± 0.3
Adhesion enthalpy ($mN\ m^{-1}$)	−6.5 ± 1.4	−3.7 ± 1.2	−1.7 ± 1.5	−13.8 ± 2.3
Entropic contribution ($mN\ m^{-1}$)	−5.5 ± 1.8	−2.6 ± 1.8	−1.2 ± 1.6	−9.8 ± 2.5
Hydrogen bond density (nm^{-2})	6.28 ± 0.01	8.65	7.41 ± 0.03	8.15 ± 0.01

B. Titania-bilayer interface

The adsorbed bilayers are characterized by various properties listed in Tables III and IV. Although the bilayers spontaneously adhered to all the surfaces, evidenced by the negative values of the bilayer adhesion strength, there was a marked amount of variation in the magnitude of the adhesion strength. The adhesion was particularly strong on the rutile 101 and anatase 110 surfaces at −4.0 ± 0.5 mN m^{-1} and −4.0 ± 0.3 mN m^{-1}, respectively. The rutile 001 and anatase 001 surfaces, on the other hand, exhibited relatively weak adhesion with values of only −0.3 ± 0.1 mN m^{-1} and −0.6 ± 0.2 mN m^{-1}.

Additional properties are measured through the central section of the adhering bilayer (see Fig. 3). The width of this region was determined by observation of the lipid surface density, expressed as the projected area per lipid (ApL), as a function of distance from the ribbon edge. The region over which this property was constant was inferred to be a representative of a macroscale supported lipid bilayer. Free bilayers are observed[33] to have an ApL of 0.62 nm^2, and this represents the lower limit of the time averaged ApL measured on the various surfaces in this study. The greatest deviation from this value was 0.66 nm^2, measured on the rutile 101 surface.

Partial number density profiles, measured through the central section of the adhering membrane, are shown in Figs. 4 and 5. The profiles are divided into contributions from the lipid head, lipid tails, and the water phase, excluding all hydrogen atoms. The lipid head atoms include atoms in the choline, phosphate, and glycerol moieties as well as atoms in the carboxyl group of the palmitic acid tail. All the remaining carbon atoms in the lipid molecule contribute to the lipid tail profile.

Additional parameters characterizing the supported lipid bilayer (SLB) are the separation and the thickness. The former is measured along the surface normal between the surface, located at the mean position of the superficial titanium atoms, and the time averaged mean position of the atoms constituting the previously defined head group adjacent to the surface. Similarly, the thickness is measured between the time averaged mean positions of the head group in each leaflet. Note that this definition for the thickness does not allow for direct comparison with empirically determined

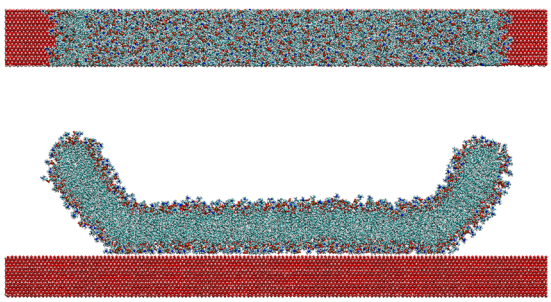

FIG. 3. Top and side views of a lipid ribbon adsorbed on the rutile 100 surface. Water is omitted for clarity.

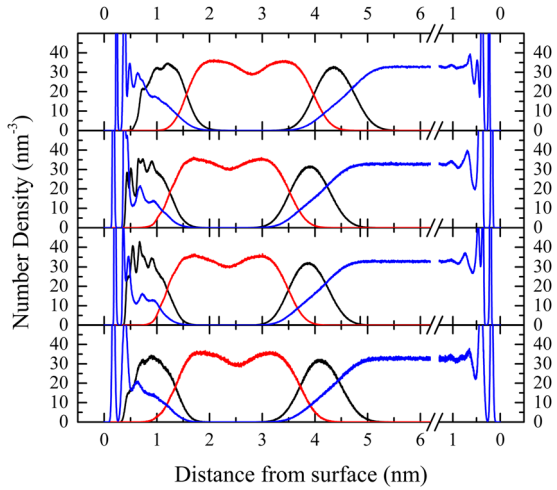

FIG. 4. Number density profiles across the central section of the adsorbed bilayer on the rutile surfaces. The origin on the abscissa corresponds to the average position of the superficial titanium atoms. The right-hand side shows density profiles near the nonadsorbing surface. Black: lipid head group atoms. Red: lipid tail group atoms. Blue: water molecules. From top: 110, 100, 101, and 001.

values of bilayer thickness based on small-angle neutron scattering and will give a value of approximately 3.2 nm for the thickness of a free bilayer.[36] The separations range from 0.81 nm on the anatase 110 surface to 1.53 nm on the anatase 100 surface. This range is generally greater than the separations observed on the silica surfaces, which ranged from 0.52 nm to 0.76 nm (the exception being the dehydroxylated, and consequentially hydrophobic, Q^4 surface with 1.01 nm separation). This comparison is borne out by observation of the partial density profiles in Figs. 4 and 5, which show that in

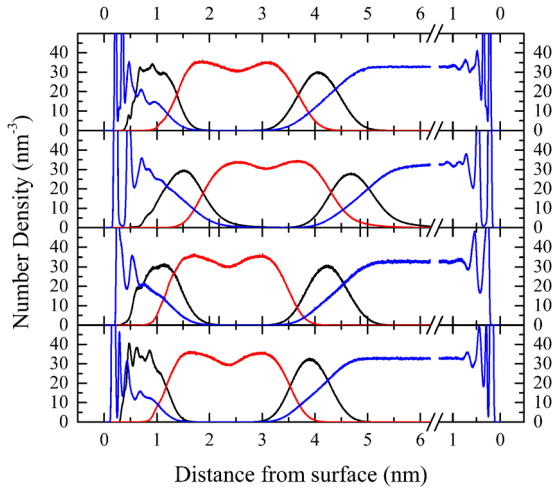

FIG. 5. Number density profiles across the central section of the adsorbed bilayer on the anatase surfaces. The origin on the abscissa corresponds to the average position of the superficial titanium atoms. The right-hand side shows density profiles near the nonadsorbing surface. Black: lipid head group atoms. Red: lipid tail group atoms. Blue: water molecules. From top: 101, 100, 001, and 110.

general the first two layers of water remain intact when the bilayer adheres to the titania surfaces. In contrast, adhering bilayers on silica surfaces penetrate the surface water layer to directly contact the silica surface. The thickness of the SLB ranges from 3.03 nm on the rutile 100 surface to 3.22 nm on the anatase 100 surface, the latter being comparable to the thickness of a free bilayer. Note that in general, surfaces with strong adhesion tend to exhibit adhering bilayers with greater ApL, smaller separation, and smaller thickness. This is in agreement with the general relationship between these SLB characteristics and adhesion strength observed in the silica and gold studies although the correlation is not as strong across all the surfaces in this study.

Bilayer adhesion enthalpies per unit area on each surface are also included in Tables III and IV. Estimations were obtained from fully periodic simulations of each surface with a bilayer. In this geometry, the ApL of the bilayer and the amount of water intervening between the surface and bilayer are determined from the initial configuration; these properties are constrained by the periodic boundary conditions. For each surface, two simulations were performed. The first was with a bilayer in contact with the surface such that the ApL and the intervening water match as closely as possible the values observed in the ribbon simulations as recorded in the relevant tables. The second simulation had exactly the same amount of water and lipids, but the bilayer was located in the middle of the water channel separating periodic images of the surface. The difference in the total enthalpy between the two simulations divided by the projected surface area determines the adhesion enthalpy per unit area.

The adhesion enthalpy data indicate that adhesion on the rutile surfaces appears to be endothermic, while on the anatase surfaces, the process is exothermic. Application of the Gibbs free energy equation allows the inference of the entropic contributions to the free energy of adhesion, $T\Delta S$, for each surface. They indicate that entropy is driving adhesion on the rutile surfaces and opposing adhesion on the anatase surfaces although it is impossible to definitively conclude that the entropic contribution on the anatase 001 surface is negative as the uncertainty encompasses both positive and negative values. Unfortunately, we have been unable to construct a convincing molecular level explanation for this curious phenomenon.

Finally, we calculated the time averaged number of hydrogen bonds, per unit area, between the titania and the intervening water in the presence of the adhering bilayer. Note that the hydrogen bond density was effectively constant across the simulation time span, so as a consequence, no errors are reported. There are four surfaces where there was a small but significant decrease in the hydrogen bond surface density when the bilayer adheres: rutile 100, rutile 101, rutile 001, and anatase 110. These represent the surfaces with the greatest hydrogen bond density and least separation between the surface and bilayer. Additionally, the density profiles show that there is significant penetration of the second water layer adjacent to the surface, suggesting that the bilayer is disrupting the formation of hydrogen bonds between the titania and the secondary water layer.

IV. CONCLUSIONS

In this paper, we detail computational estimates of the adhesion strength of DMPC bilayers on a variety of titania surfaces,

representing four low-energy cleavage planes of each polymorph. The average adhesion strength across the cleavage planes for rutile and anatase is relatively weak at ∼−2.0 ± 0.4 mN m^{-1}. However, rutile has two (100 and 101) high energy surfaces (−4 mN m^{-1}), while anatase has only one (110). Since particle surfaces are expected to comprise a range of low energy cleavage planes, this observation suggests a slightly greater tendency for bilayers to wrap rutile particles compared to anatase particles, but both forms wrap less than amorphous silica. The adhesion mechanism between the polymorphs also appears to differ—the entropic contribution to the adhesion free energy appears to drive adhesion on the rutile surfaces and oppose adhesion on the anatase surfaces.

Computational bilayer adhesion studies have now been conducted on three materials, gold, silica, and titania, which collectively exhibit a spectrum of adhesion characteristics. We have attempted to correlate the adhesion strength with other properties—such as immersion enthalpy and single lipid adsorption free energy—that are easier to measure. However, the only generally reliable predictor of adhesion strength appears to be the equilibrium separation between the bilayer and surface. Gold displays very strong adhesion, characterized by a separation of 0.33 nm between the substrate and bilayer head group, with a strength of −40 mN m^{-1}. Silica has a maximum adhesion strength of −7.5 mN m^{-1} at a separation of 0.52 nm[17] on the amorphous Q^{3a} surface, and titania has a maximum strength of −4.0 mN m^{-1} at a separation of 0.85 nm on the rutile 101 surface and 0.81 nm on the anatase 110 surface. Bilayers adhere to other low surface energy cleavage planes of these metal oxides less strongly. The relative adhesion strengths of these materials are consistent with reports of low toxicity for titania.[25] Yu *et al.*[28] reported markedly stronger adsorption of PE on rutile than on anatase, especially at low concentrations; our simulations predict that only rutile 101 will adsorb DMPC significantly at low concentrations. It remains to be seen if there is a significant difference between the adsorption of PC and PE.

SUPPLEMENTARY MATERIAL

See the supplementary material for all input files and analysis scripts necessary to run simulations with GROMACS which are included in a gzip archive. Configuration files in gro format are taken from the end of our simulation trajectories.

ACKNOWLEDGMENTS

We acknowledge funding from the European Union's Horizon 2020 research and innovation program under Grant Agreement No. 686098, "Smartnanotox," and access to supercomputing facilities though the ARCHER UK National Supercomputing Service.

REFERENCES

[1] M. Sajid, M. Ilyas, C. Basheer *et al.*, "Impact of nanoparticles on human and environment: Review of toxicity factors, exposures, control strategies, and future prospects," Environ. Sci. Pollut. Res. **22**(6), 4122–4143 (2015).
[2] F. Joris, B. B. Manshian, K. Peynshaert *et al.*, "Assessing nanoparticle toxicity in cell-based assays: Influence of cell culture parameters and optimized models for bridging the *in vitro–in vivo* gap," Chem. Soc. Rev. **42**(21), 8339–8359 (2013).
[3] N. Lewinski, V. Colvin, and R. Drezek, "Cytotoxicity of nanoparticles," Small **4**(1), 26–49 (2008).
[4] L. Yildirimer, N. T. K. Thanh, M. Loizidou *et al.*, "Toxicology and clinical potential of nanoparticles," Nano Today **6**(6), 585–607 (2011).
[5] K. Yamashita, Y. Yoshioka, K. Higashisaka *et al.*, "Silica and titanium dioxide nanoparticles cause pregnancy complications in mice," Nat. Nanotechnol. **6**(5), 321–328 (2011).
[6] F. Gottschalk and B. Nowack, "The release of engineered nanomaterials to the environment," J. Environ. Monit. **13**(5), 1145–1155 (2011).
[7] A. Nel, T. Xia, L. Mädler *et al.*, "Toxic potential of materials at the nanolevel," Science **311**(5761), 622–627 (2006).
[8] See http://smartnanotox.scientia.global/ for information about the smartnanotox project.
[9] See https://www.nanosafetycluster.eu/ for EU NanoSafety cluster – about the NanoSafety cluster.
[10] K. Kettler, K. Veltman, D. van de Meent, A. van Wezel, and A. J. Hendriks, "Cellular uptake of nanoparticles as determined by particle properties, experimental conditions, and cell type," Environ. Toxicol. Chem. **33**, 481–492 (2014).
[11] R. Michel, E. Kesselman, T. Plostica, D. Danino, and M. Gradzielski, "Internalization of silica nanoparticles into fluid liposomes: Formation of interesting hybrid colloids," Angew. Chem., Int. Ed. **53**, 12441–12445 (2014).
[12] Y. Roiter, M. Ornatska, A. R. Rammohan, J. Balakrishnan, D. R. Heine, and S. Minko, "Interaction of nanoparticles with lipid membrane," Nano Lett. **8**, 941–944 (2008).
[13] W. Helfrich, "Elastic properties of lipid bilayers: Theory and possible experiments," Z. Naturforsch., C **28**(11), 693 (1973).
[14] M. Deserno and W. M. Gelbart, "Adhesion and wrapping in colloid–vesicle complexes," J. Phys. Chem. B **106**(21), 5543–5552 (2002); See also M. Deserno, "Elastic deformation of a fluid membrane upon colloid binding," Phys. Rev. E **69**, 031903 (2004).
[15] C. Contini, M. Schneemilch, S. Gaisford, and N. Quirke, "Nanoparticle–membrane interactions," J. Exp. Nanosci. **13**(1), 62–81 (2018).
[16] M. Schneemilch and N. Quirke, "Free energy of adsorption of supported lipid bilayers from molecular dynamics simulation," Chem. Phys. Lett. **664**, 199–204 (2016).
[17] M. Schneemilch and N. Quirke, "Free energy of adhesion of lipid bilayers on silica surfaces," J. Chem. Phys. **148**(19), 194704 (2018); Erratum, **150**, 229901 (2019).
[18] A. Weir, P. Westerhoff, L. Fabricius, K. Hristovsk, and N. von Goet, Environ. Sci. Technol. **46**(4), 2242–2250 (2012).
[19] R. Liu, X. Zhang, Y. Pu, L. Yin, Y. Li, X. Zhang, G. Liang, X. Li, and J. Zhang, "Small-sized titanium dioxide nanoparticles mediate immune toxicity in rat pulmonary alveolar macrophages *in vivo*," J. Nanosci. Nanotechnol. **10**(8), 5161–5169 (2010).
[20] B. Trouiller, R. Reliene, A. Westbrook, P. Solaimani, and R. H. Schiestl, "Titanium dioxide nanoparticles induce DNA damage and genetic instability *in vivo* in mice," Cancer Res. **69**(22), 8784–8789 (2009).
[21] K. Bhattacharya, M. Davoren, J. Boertz, R. Schins, E. Hoffmann, and E. Dopp, "Titanium dioxide nanoparticles induce oxidative stress and DNA-adduct formation but not DNA-breakage in human lung cells," Partical Fiber Toxciology **6**, 17 (2009).
[22] M. Setyawati *et al.*, "Titanium dioxide nanomaterials cause endothelial cell leakiness by disrupting the homophilic interaction of VE-cadherin," Nat. Commun. **4**, 1673 (2013).
[23] J. A. Jackman, G. H. Zan, Z. Zhao, and N.-J. Cho, Langmuir **30**, 5368–5372 (2014).
[24] F. Wang and J. Liu, J. Am. Chem. Soc. **137**, 11736–11742 (2015).
[25] C.-H. Wu, "Physiochemical characteristics contributing to the cytotoxicity of transition metal oxides," M.Sc. thesis, Missouri University of Science and Technology, 2012, p. 5208, https://scholarsmine.mst.edu/masters_theses/5208.
[26] I. Urbančič *et al.*, Nano Lett. **18**, 5294–5305 (2018).
[27] A. Vakurov, R. Drummond-Brydson, O. Ugwumsinachi, and A. Nelson, "Significance of particle size and charge capacity in TiO_2 nanoparticle-lipid interactions," J. Colloid Interface Sci. **473**, 75–83 (2016).

[28]Q. Yu, H. Wang, Q. Peng, Y. Li, Z. Liu, and M. Li, J. Hazard. Mater. **335**, 125–134 (2017).
[29]E. G. Brandt and A. P. Lyubartsev "Force field development by partitioning electron densities on atomistic neighborhoods: The TiO_2-water interface" (unpublished).
[30]L. Agosta, E. G. Brandt, and A. P. Lyubartsev, "Diffusion and reaction pathways of water near fully hydrated TiO_2 surfaces from *ab initio* molecular dynamics," J. Chem. Phys. **147**(2), 024704 (2017).
[31]T. R. Esch, I. Gadaczek, and T. Bredow, "Surface structures and thermodynamics of low-index of rutile, brookite and anatase—A comparative DFT study," Appl. Surf. Sci. **288**, 275–287 (2014).
[32]J. P. M. Jämbeck and A. P. Lyubartsev, "Derivation and systematic validation of a refined all-atom force field for phosphatidylcholine lipids," J. Phys. Chem. B **116**(10), 3164–3179 (2012).
[33]J. P. M. Jämbeck and A. P. Lyubartsev, "An extension and further validation of an all-atomistic force field for biological membranes," J. Chem. Theory Comput. **8**(8), 2938–2948 (2012).
[34]J. P. M. Jämbeck and A. P. Lyubartsev, "Another piece of the membrane puzzle: Extending slipids further," J. Chem. Theory Comput. **9**(1), 774–784 (2013).
[35]J. S. Hub, B. L. de Groot, and D. van der Spoel, "g wham—A free weighted histogram analysis implementation including robust error and autocorrelation estimates," J. Chem. Theory Comput. **6**(12), 3713–3720 (2010).
[36]Scattering experiments typically rely on models of the bilayer comprising parallel strips of constant density to compute the bilayer thickness, which are more akin to the distance between the two lipid-water phase boundaries. For example, using the water profile half-height gives values around 3.5 nm, while use of the lipid density half-height will give values closer to 4.5 nm. In our application, the leaflet at the surface is often highly structured (such as for rutile 100) and has varying degrees of water penetration or—in the case of very strongly adhering surfaces—little intervening water at all. This makes the molecular-scale definition of the phase boundary location problematic, so we have adopted a more straightforward definition that can be applied unambiguously to allow comparison between simulations over a wide range of adhesion strengths.